Planning Routes of Continuous Illumination and Traversable Slope using Connected Component Analysis*

Nathan D. Otten[1], Heather L. Jones[1], David S. Wettergreen[1], and William L. Whittaker[1]

***Abstract*— This paper presents a method that applies connected component analysis to plan routes that keep robots continuously illuminated and on traversable slopes while reaching one or more goal locations. Such routes promise to extend the lifespan, range, and scientific return of solar-powered robots exploring environments with changing but predictable lighting conditions, particularly those of the Moon and Mercury. Maps of lighting and ground slope that describe these constraints in position and time are computed, and all distinct interconnected regions that have both direct sunlight and safe slope are found using connected component analysis. These three-dimensional connected components are pruned of roots that violate time constraints and branches that dead-end in discontinuous routes. Each component is the basis for a graph that includes all feasible routes from the initial time to the final time of that component. The shortest feasible route between a pair of start and goal positions within the same component is found using A* search and is characterized by its total length and average speed. Malapert Peak and Shackleton Crater, both near the Moon's South Pole, serve as examples throughout this paper due to their highly-relevant, dynamic, and predictable lighting caused by the Moon's motion relative to the Sun.**

I. INTRODUCTION

Planetary rovers encounter changing illumination and are challenged to generate and maintain adequate power to function while navigating hazardous terrain. Lighting, temperature, and available communication all vary temporally due to planetary tilt, orbit, and rotation, which lead to the ever-changing insolation conditions on the surface. On the Moon, sunlight varies periodically on a month-long diurnal cycle and evolves more subtly on an annual cycle. These variations are amplified at the pole, where lower sun angles generate longer shadows. Fluctuations in solar illumination induce equally dramatic swings in surface temperature, particularly on airless bodies like the Moon and Mercury with no appreciable atmosphere. At night, lunar surface temperatures plunge below 100 K (-173 °C) [1], [2], and daytime temperatures reach 390 K (117 °C) at the equator [1], [3].

Solar-powered rovers that cannot keep pace with the Sun will thus experience intermittent power and extreme temperatures and will be subject to the cold, dark night, which lasts more than 14 Earth days on the Moon and 88 Earth days on Mercury. A rover design that utilizes only solar energy and can tolerate the full spectrum of observed temperatures has yet to be achieved, and currently practical battery capacities are insufficient to accommodate both extremes. Prior lunar rover missions have mitigated extreme temperatures by avoiding the hottest environments on the Moon and by using scarce nuclear isotopes to generate heat at night, but at great cost in terms of money, time, and mass. Even with nuclear heating, these rovers were forced to cease operation and hibernate through the darkness, hampering their missions of exploration.

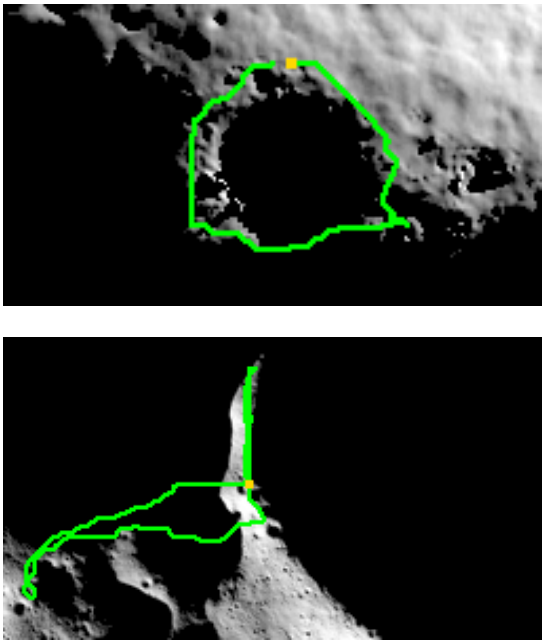

Fig. 1: Nomadic exploration routes at Malapert Peak (top) and Shackleton Crater (bottom) near the Lunar South Pole. These static views, shown projected onto one snapshot of illumination conditions, give the false impression that the routes cross shadow; however, a rover following this route (defined in x, y, and t) remains illuminated at all times. See the accompanying video for a better visualization.

This research introduces a roving strategy called *nomadic exploration* that follows the ever-shifting regions of solar power, moderate temperatures, and reliable communication. Sun-synchronous circumnavigation routes that circle geographic features to maximize solar power have previously been envisioned [4] and partially demonstrated [5] but without Moon- or Mercury-relevant lighting. This behavior could

*This work was supported by NASA Innovative Advanced Concepts (NIAC) Program grant NNX13AR25G, John Falker, Program Executive; NSF Graduate Research Fellowship Program grant DGE1252522; and NASA Space Technology Research Fellowship grant NNX12AM43H.

[1]The Robotics Institute, Carnegie Mellon University, Pittsburgh, PA 15213, USA {otten, heatherljones, dsw, red}@cmu.edu

be applied around small, local geographic features (e.g., mountain peaks near the Lunar poles), mid-sized regions (e.g., large polar craters), or global routes (e.g., the equatorial circumference of the Moon or Mercury). The primary distinction between these scenarios is the speed required to complete the circuit and the amount of time available for performing experiments and collecting scientific data. Circling a 200-meter-diameter peak or crater near the Moon's pole while remaining in sunlight requires an average speed of only about 1 meter per hour. This is approximately 10% of the Mars Exploration Rover's overall drive speed [6]. This type of repetitive local route provides opportunities for densely distributed science sampling over a long period of time. Traveling faster enables exploration of larger regions and forays to more diverse science targets. These local and regional routes are the primary attention of this paper, in which Malapert Peak and Shackleton Crater near the Lunar South Pole serve as examples (Fig. 1). At the other extreme, circumnavigating the Moon's equator in a single lunar period requires an average speed of about 16 kilometers per hour, which is about the maximum velocity of the Apollo Lunar Roving Vehicle [7].

Nomadic exploration offers substantial benefits to a solar-powered rover's range and life span but complicates route planning. This paper describes and demonstrates a route planning architecture that utilizes connected component analysis to plan nomadic routes that never pass through shadows or over steep terrain but instead provide continuous illumination and traversable slope.

II. MAPS

A model of illumination with respect to time provides a basis for reasoning about available power and thermal conditions. The process of creating illumination maps for this work starts with high-resolution elevation data. For the Moon, the source is the NASA Lunar Reconnaissance Orbiter (LRO) satellite's Lunar Orbiter Laser Altimeter (LOLA) instrument, for which gridded data has been compiled down to 5 meter-per-pixel resolution close to the pole (Fig. 2a), and the Narrow Angle Camera (NAC), for which down to 2 meters per pixel has been achieved from stereo processing, where images exist. For areas farther from the pole, the best available resolution decreases due to the limited coverage of the polar-orbiting LRO.

High-resolution digital elevation map (DEM) data is used to build a mesh model of terrain that lies within the illumination map (Fig. 2b). To do this, the map projection of the DEM data, (often polar stereographic), must be reversed to get 3D terrain points. This ensures that the model will be the right shape to interact realistically with incident illumination, including effects due to a planetary body's curvature; capturing curvature effects is important when determining lighting and shadows.

The terrain within the map's image frame does not completely determine the illumination in the image. Large terrain features outside the image frame can also cast shadows into the frame. Thus, the model used for computing illumination

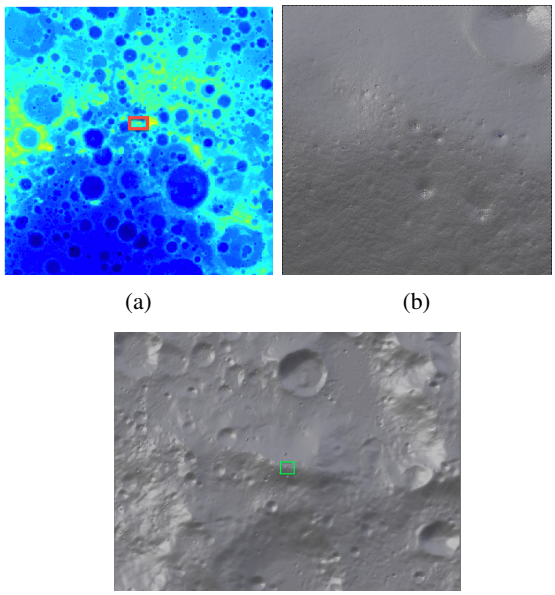

(a) (b)

(c)

Fig. 2: (a) A DEM of the Moon's South Pole out to 60 degrees south built from LOLA data [8]. The red box indicates the position of the terrain shown in Fig. 2c. (b) Mesh model of terrain for Malapert Peak. (c) Mesh model of Malapert Mountain showing a high-resolution model in the frame to be rendered (that of Fig. 2b) and a lower-resolution model of the wider area.

needs to be much wider than the image frame. The necessary size of the wider model is calculated considering the curvature of the Moon and the elevation of terrain features. The immediate border of the image frame is modeled using high-resolution data, but the wider region outside the image frame is modeled using lower resolution data. This is done both to reduce memory requirements and because high-resolution data is often not available for the entire wide area. A mesh model with high-resolution and low-resolution segments is shown in Fig. 2. This model is created using a high-resolution stereo DEM at 2 meters per pixel [9], a medium-resolution LOLA DEM at 10 meters per pixel to fill gaps in the stereo data [10], and a low-resolution LOLA DEM at 240 meters per pixel to capture the wider region [8].

To model solar illumination, the SPICE toolkit [11] is used to find the location of the Sun and the location of a point in the center of the image frame at each time of interest. From this, a Sun vector in the local frame is computed.

Once the terrain model and illumination are known, this information is rendered using a ray tracing algorithm [12], [13], producing an orthographic projection into the image frame. The resolution of the illumination map is selected to be half the resolution of the mesh model so that individual triangles in the mesh are not visible in the illumination image (Fig. 3).

The rendered illumination images are converted to binary maps using a threshold intensity value below which pixels are considered unlit, or shadowed. These pixels are set to

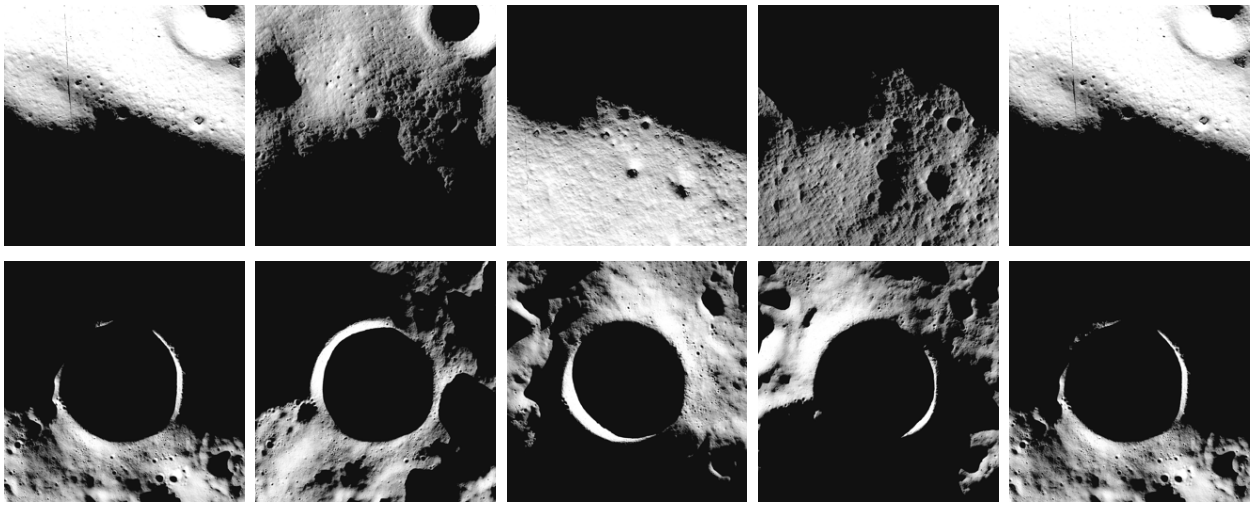

Fig. 3: Simulated illumination-maps of Malapert Peak (top) and Shackleton Crater (bottom) spanning one month.

0. Pixels with intensities above this threshold are set to 1 and considered to be illuminated with adequate sunlight to power photovoltaic cells on a rover's solar panel. Brightness in the rendered image is an approximation of solar intensity because the optical properties of the terrain material are constant across the model; color (albedo) variations of the terrain are not included, so image brightness depends solely on the interaction of the terrain geometry with incident light, and the rendering does not include indirect lighting. For the examples presented here, the threshold was set at 0, so all nonzero illumination is defined as lit, and everything else is defined as shadowed. This assumes that any positive amount of solar illumination is adequate to fully power the rover, which is true for rover configurations with two-degree-of-freedom articulated solar arrays that can always point directly at the sun (provided the array is appropriately sized).

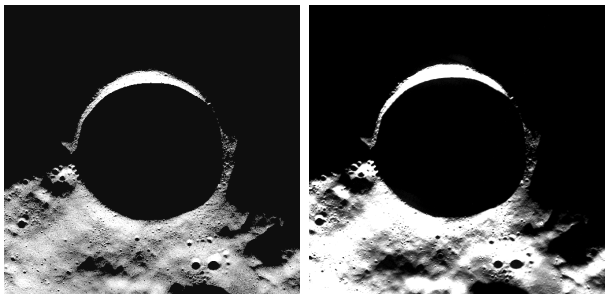

Fig. 4: Rendered image of Shackleton Crater (left) and image of Shackleton Crater taken by the LRO's Wide Angle Camera (right) for the same time, showing correspondence between the simulated and actual lit areas [14].

To validate the simulation of illumination, images were rendered of Shackleton Crater for times corresponding to three images from the LRO's Wide Angle Camera (WAC) [14], [15], [16]. Each image was map-projected to a polar stereographic projection using USGS's ISIS tool (the WAC is a pushframe camera, so raw images are not trivial to interpret before map projection) [17]. Some differences between rendered images and actual data were noted, including hard versus soft shadows and differences in image intensity due to the reflectance model used for rendering, but generally the match was accurate (Fig. 4).

In addition to illumination, this route planning architecture considers terrain traversability by creating a map of surface slopes. Small, rover-scale obstacles such as rocks and craters less than a few meters across are not observable by LRO's instruments due to limited resolution, so these hazards cannot be planned for based on existing satellite data. Local slopes, however, can be calculated from the same terrain models used for determining illumination. The average ground slope for each pixel follows from its gradient, which is computed as a divided difference over the neighboring pixels (Fig. 5). A slope threshold can be chosen manually based on the expected mobility performance of a particular rover, and the slope map can be made binary to express safe and unsafe locations. This static slope map can be combined with each time slice of the illumination map to yield a binary array representing the locations and times that are both illuminated and have safe slope (Fig. 6).

III. CONNECTED COMPONENTS

This approach uses connected component analysis to find the largest interconnected regions in space and time that are continuously lit and have safe slope. These regions can be thought of as volumes in x, y, and t made up of gridded cells, or voxels. Using a flood-fill algorithm [18], we generate a sorted list of the largest connected regions in the 3D sequence of combined light-and-slope maps. The basic steps used to find the connected components are outlined in Algorithm 1. Connectivity is defined by a $3\times3\times3$-element kernel of 1s and 0s, where the center element (always 1-valued) represents the cell being examined at each iteration within flood-fill algorithm, and each neighboring element is 1-valued only if its position relative to the center element is considered connected. For example, if only the six elements sharing a face with the center element are 1-valued, then each cell is

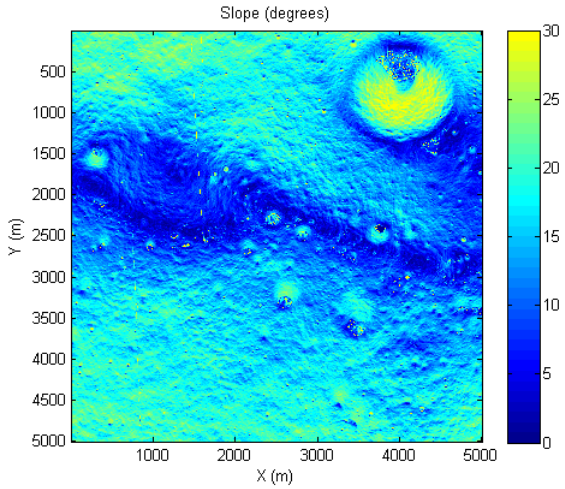

Fig. 5: Slope map for Malapert Peak region.

directly connected to just the six cells immediately adjacent to it (called the 6-connected neighborhood), and flood-fill adds those with value 1 to the same component as the central cell. The kernel is then applied to these newly added cells recursively until no new connected cells are found, which happens when the component has filled the volume bounded by 0-valued cells. Since the 27-element kernel must be symmetric about its center, there are 2^{13} possible definitions of connectivity for a 3D space. In the examples presented here, the most liberal definition of connectivity is used, in which all 26 neighboring elements are considered connected to the central element (also called the 26-connected neighborhood).

Algorithm 1 Connected Components Algorithm

Initialize all cells in Map to unlabeled
while $\exists$ unlabeled 1-valued cells $\in Map$ **do**
    $c_{seed} \Leftarrow$ next unlabeled 1-valued cell in Map
    Set $label(c_{seed}) \Leftarrow$ a unique label l
    $C \Leftarrow$ FLOODFILL3D(c_{seed})
    Set $label(c) \Leftarrow l \ \forall c \in C$
end while
function FLOODFILL3D($seed$)
    return the set C of all cells connected to $seed$
end function

Each distinct component returned by flood-fill represents an undirected graph that can subsequently be searched using standard methods such as Dijkstra's or A*. By definition, no component is connected to any other component. The vast majority of components are extremely short-lived, lasting only a few hours on the Moon, but, in the case of the Malapert and Shackleton examples (beginning in May 2015 and April 2018, respectively), one component spans the two full lunar cycles analyzed (Fig. 6). Searching just the single largest component (longest in the t-dimension) can substantially reduce the size of the graph to be searched, since all other regions can be ignored.

IV. PRUNING

Because the flood-fill algorithm's definition of connectivity must be symmetric, it produces regions that, to be reached, would require the rover to travel backward in the time dimension. This happens when two previously disconnected patches of light converge to one connected patch. If a rover starts in one of the two converging patches, it can never reach the other, despite the appearance of connectivity in three dimensions. To eliminate these features which can never be part of a feasible route, each component is pruned of branches that extend backward in time (i.e., roots) using the procedure outlined in Algorithm 2. The resulting component is a tree-like structure that only branches forward in time. The existence of a connected component that spans from t_0 to t_n indicates that a feasible continuously lit route with safe slope exists from beginning to end. In other words, a rover that starts within this lit region at t_0 can reach t_n without ever leaving the sunlight, crossing a shadow, or encountering an unsafe slope, provided that the rover has adequate speed. The absence of such a component indicates that no such path from t_0 to t_n exists.

Algorithm 2 Pruning Algorithm

Let X: number of cells in Map in the x dimension
Let Y: number of cells in Map in the y dimension
Let N: number of cells in Map in the t dimension
Let $c(x, y, t)$: cell at position (x, y) and time t
Let $Map(t)$: 2D slice of Map at time t
$\{C_0^1 ... C_m^1\} \Leftarrow$ FLOODFILL2D($Map(t)$)
Choose $C_k^1 \in \{C_0^1, ..., C_m^1\}$
Set $label(c) \Leftarrow l \ \forall c \in C_k^1$
for $i = 2...N$ **do**
    $\{C_0^i ... C_m^i\} \Leftarrow$ FLOODFILL2D($Map(t)$)
    for Each component $C \in \{C_0^i ... C_m^i\}$ **do**
        if $\exists c(x, y, i) \in C \mid label(c(x, y, i-1)) = l$ **then**
            $label(c) \Leftarrow l \ \forall c \in C$
        end if
    end for
end for
function FLOODFILL2D($slice_t$)
    return the set of all connected components $\{C_0^t, ..., C_m^t\}$ in $slice_t$
end function

If a target time-duration is known, then searching branches that do not reach that tree depth is wasteful. This can be avoided by pruning all branches but those that reach the target depth. Alternately, if there is no target time but the absolute longest possible duration is desired, then all but the deepest branch(es) can be pruned. This effectively eliminates all possible dead ends that occur when lit surface patches diverge into multiple separate regions as time advances and one or more of these regions does not reach the goal time. To implement this second stage of pruning, the result of the first pruning can be flipped in the time dimension and run through the same pruning procedure (Algorithm 2). This produces

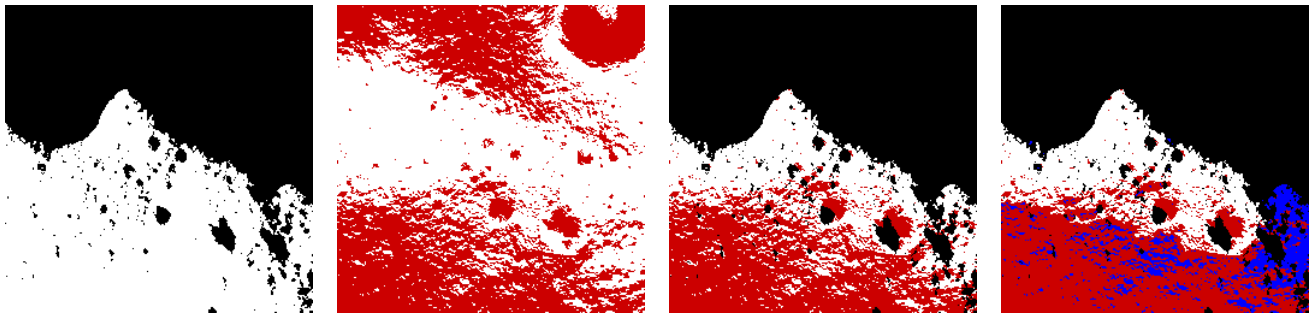

Fig. 6: From left to right: binary lighting map, binary slope map, combined slope + lighting map, and the largest connected component, all shown for just a single time step of the Malapert Peak sequence. Black is shadowed, white is lit, red is steep slope, and blue is unconnected to the largest component.

a single continuous corridor through time with no roots or branches that dead-end (Fig. 7). As long as the rover path stays within the boundaries of this corridor, it will reach t_n.

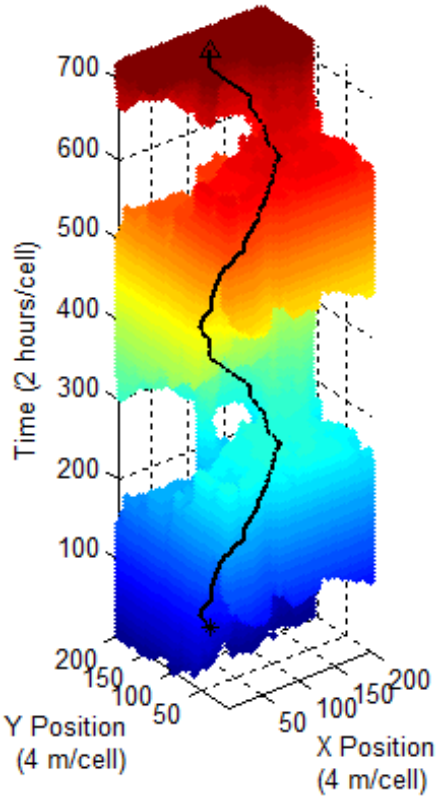

Fig. 7: 3D representation of the largest pruned component from the Malapert Peak example and resulting shortest route.

V. PATH PLANNING

Once pruned, the continuously illuminated component is used as a graph for planning routes between any two points that lie within the component. Of most interest are the routes that start at t_0 and end at t_n, since the goal is to extend rover operation as long as possible. Each 1-valued cell in the pruned component represents a graph node, and edges are defined between neighboring nodes in the same sense as connectivity in Section III except that all edges are directed forward in time. That is, each node is connected only to the 9 neighboring nodes in the following time step and is not connected to any nodes in the same or previous time steps. With each action, the search algorithm moves exactly one cell forward in time and a maximum of one cell in each of the x and y directions. Utilizing connected components to generate a graph structure in this way need not be restrictive to this type of movement, however. If the rover is fast enough, multiple moves in $x-y$ can be made within a single time step in a manner similar to [19].

Standard A* search was used to find the shortest route between starting locations at t_0 and goal locations at t_n, where distance was defined by the Euclidean norm. Example routes computed in this way using several intermediate waypoints are shown in Fig. 8.

The Malapert and Shackleton routes travel a total distance of 2.16 and 34.7 kilometers, respectively, over two full lunar cycles (59 Earth days), resulting in an average speed of 1.5 and 25 meters per hour, respectively. The Malapert and Shackleton routes also feature respective maximum dwell times when the rover is stationary for up to 45 and 226 consecutive hours. Long dwell times are desirable to facilitate scientific experiments and data collection at points of interest while still remaining in constant sunlight. Future work will optimize these dwell times and locations to maximize scientific return.

VI. CONCLUSIONS

This paper presents a route planning method that uses connected components to enforce spatiotemporal constraints, specifically lighting and slope. As a specific example, connected component analysis was applied to 3D illumination and slope maps of the Malapert Mountain and Shackleton Crater regions near the Moon's South Pole to plan enduring routes that are continuously illuminated and of traversable slope. Sun-synchronous circumnavigation eliminates the need for hibernation through the lunar night, and constant solar power multiplies the amount of exploration, science, and utility that is possible. A solar-powered rover exploring environments like the lunar poles with predictable but dynamic lighting must consider not just where it needs to

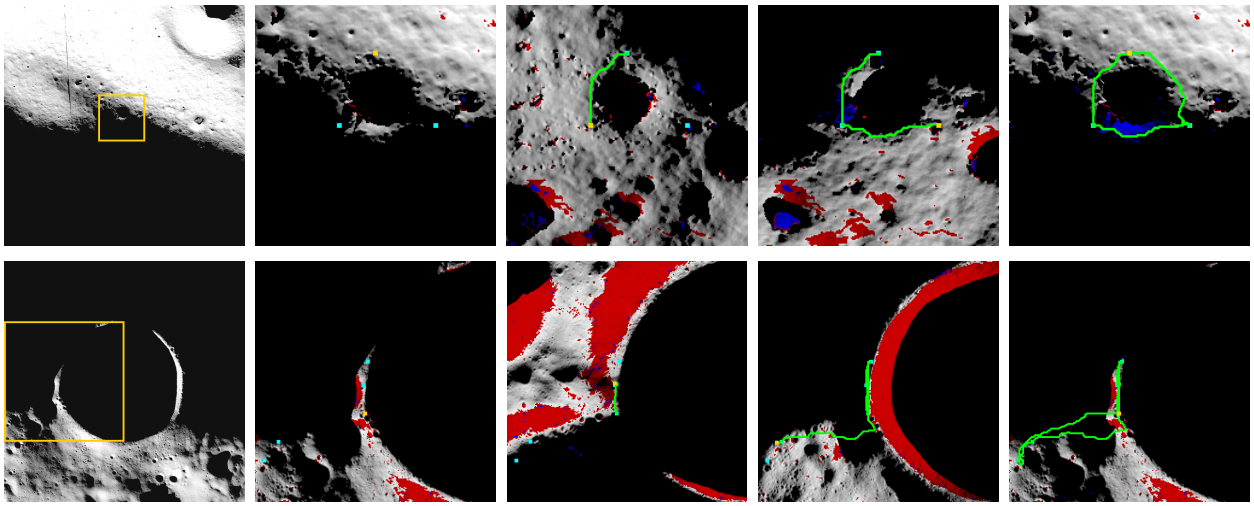

Fig. 8: Planned route shown at several time steps during one lunar cycle for Malapert (top) and two lunar cycles for Shackleton (bottom). The leftmost image in each row indicates the area of the larger map shown in the following images. Red indicates high slope, and blue indicates disconnected regions. The route is green, and waypoints are cyan.

be to achieve its mission but also when it needs to be there. Technology that enables this kind of temporal constraint reasoning will be vital to exploring such areas.

Future work will consider not just lighting and slope, but also temperature and communication, as these constraints are crucial to effective extended operation. Communication visibility to Earth can be modeled nearly identically to sunlight. Although A* search can find the optimal route (shortest, fastest, or otherwise), it is still computationally prohibitive at high resolutions and large scales. Hierarchical approaches address this problem by decomposing it into a series of local searches at varying resolutions. This improves performance but at the cost of optimality.

For missions that explore resources at the lunar poles, route planning will need to incorporate reasoning about rover power levels to enable limited forays into permanently dark craters to measure the frozen water that lies within. Long dwell times in illuminated locations are desirable to perform science experiments and data collection but must not cause the rover to fall behind and become trapped in shadow with no power source. Routes will need to be optimized for combinations of desirable metrics including average speed, maximum speed, average and maximum slope, risk of becoming stranded in shadow, and long dwell times.

References

[1] D. Paige. (2014, May) DIVINER lunar radiometer experiment: The lunar thermal environment. AbFab_Plot.png. [Online]. Available: http://www.diviner.ucla.edu/science.shtml

[2] I. Thomas, "Measurement of properties of the lunar surface using the diviner lunar radiometer experiment on the nasa lunar reconnaissance orbiter," University of Oxford," Second Year Report, Aug. 2009.

[3] A. R. Vasavada, J. L. Bandfield, B. T. Greenhagen, P. O. Hayne, M. A. Siegler, J.-P. Williams, , and D. A. Paige, "Lunar equatorial surface temperatures and regolith properties from the diviner lunar radiometer experiment," *Journal of Geophysical Research*, vol. 117, 2012, e00H18, doi:10.1029/2011JE003987.

[4] W. Whittaker, G. Kantor, B. Shamah, and D. Wettergreen, "Sun-synchronous planetary exploration," in *AIAA Space*, 2000.

[5] D. Wettergreen, P. Tompkins, C. Urmson, M. D. Wagner, and W. L. Whittaker, "Sun-synchronous robotic exploration: Technical description and field experimentation," *The International Journal of Robotics Research*, vol. 24, no. 1, pp. 3–30, January 2005.

[6] M. Maimone, Y. Cheng, and L. Matthies, "Two years of Visual Odometry on the Mars Exploration Rovers," *Journal of Field Robotics*, vol. 24, no. 3, pp. 169–186, Mar. 2007. [Online]. Available: http://doi.wiley.com/10.1002/rob.20184

[7] V. Asnani, D. Delap, and C. Creager, "The development of wheels for the Lunar Roving Vehicle," *Journal of Terramechanics*, vol. 46, no. 3, pp. 89–103, June 2009. [Online]. Available: http://www.sciencedirect.com/science/article/pii/S0022489809000263

[8] D. E. Smith, "LRO-L-LOLA-4-GDR-V1.0," Goddard Space Flight Center, LOLA Gridded Data Record Shape Map LDEM_60S_240M, 12 2013, v2.1.

[9] LROC Team, "LRO MOON LROC 5 RDR V1.0," German Aerospace Center (DLR), LROC Special Data Record NAC Digital Terrain Map NAC_DTM_ESALL_MP1, 10 2012.

[10] D. E. Smith, "LRO-L-LOLA-4-GDR-V1.0," Goddard Space Flight Center, LOLA Gridded Data Record Shape Map LDEM_85S_10M, 12 2013, v2.0.

[11] C. H. Acton, "Ancillary data services of NASA's navigation and ancillary information facility," *Planetary and Space Science*, vol. 44, no. 1, pp. 65–70, 1996.

[12] A. Keller, "Instant radiosity," in *SIGGRAPH '97 Proceedings of the 24th annual conference on Computer graphics and interactive techniques*, 1997, pp. 49–56.

[13] Blender Foundation, "Blender," www.blender.org, 2013.

[14] LRO LROC Team, "LRO-L-LROC-2-EDR-V1.0," Arizona State University, EDR M138582948ME, 10 2013.

[15] ——, "LRO-L-LROC-2-EDR-V1.0," Arizona State University, EDR M124020663ME, 9 2013.

[16] ——, "LRO-L-LROC-2-EDR-V1.0," Arizona State University, EDR M147761957ME, 10 2013.

[17] L. R. Gaddis, J. Anderson, K. Becker, T. Becker, D. Cook, K. Edwards, E. Eliason, T. Hare, H. Keiffer, E. M. Lee, J. Matthews, L. A. Soderblom, T. Sucharski, and J. Torson, "An Overview of the Integrated Software for Imaging and Spectrometers," in *Lunar and Planetary Science Conference*, 1997.

[18] V. Zammit, M. Rizzo, and K. Debattista, "CSM213 computer graphics," Department of Computer Science and A.I., University of Malta, pp. 27–29, Feb. 2001, 4.3.2 Flood-Fill Algorithm. [Online]. Available: http://staff.um.edu.mt/kurt/documents/grafx.pdf

[19] C. Cunningham, H. Jones, J. Kay, K. M. Peterson, and W. Whittaker, "Time-dependent planning for resource prospecting," in *Proc. 12th International Symposium on Artificial Intelligence, Robotics and Automation in Space*, Montreal, Canada, June 2014.